

# Optimal Galvanic Cell Design for Powering Ingestible Devices in Varying Gastrointestinal Conditions

Camden Kitchen,\* Volkan Erturk, Linhardt Ordella, Abhishek Swaminathan, and Seun Sangodoyin

Cite This: *ACS Appl. Energy Mater.* 2025, 8, 6545–6556

Read Online

ACCESS |

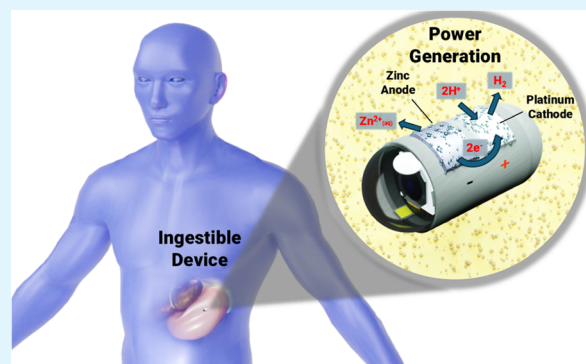
Metrics &amp; More

Article Recommendations

Supporting Information

**ABSTRACT:** Energy harvesting using galvanic cells in the gastrointestinal (GI) tract can provide supplementary power and prolong the service life of ingestible devices. This paper explores the impact of electrode type, dimension, and varying gastrointestinal (GI) conditions on the performance of galvanic cells for powering ingestible devices. *In vitro* experiments were conducted with varying cathode and anode combinations in synthetic gastric fluid (SGF) under a load resistance sweep to measure the voltage of the galvanic cell. Eighteen tests assessed the peak power, energy capacity, and longevity of each electrode pair. Galvanic cell performance was also evaluated under simulated GI conditions, including varying pH, salt concentration, added foreign substances, and simulated intestinal conditions. Pt and Pd cathodes showed the highest peak power and energy capacity, while Mo was cost-effective for transient applications. Mg was optimal for short-term use, while Zn or the AZ31B Mg alloy were preferred for long-term applications. Energy generation decreased with increasing pH but improved with higher salt concentration. Large substances in gastric fluid hindered performance, and energy generation in intestinal fluids was less efficient. Larger cathode-to-anode size ratios increased efficiency, while larger anodes provided greater longevity. This study successfully characterized the effects of electrode combinations, GI conditions, and dimensions on the performance of galvanic cells, offering insight into the design of supplementary power sources for ingestible devices. These findings aid the development of galvanic cells for short-term and long-term applications in ingestible devices.

**KEYWORDS:** energy harvesting, gastrointestinal fluid, ingestible devices, electrodes, gastrointestinal conditions



## 1. INTRODUCTION

The gastrointestinal (GI) system is essential for digestion, nutrient absorption, and defense against pathogens. Extending from the mouth to the anus, it involves coordinated muscle activity, enzymes, and interactions with the immune and nervous systems. Common disorders, such as Crohn's disease, celiac disease, polyposis syndrome, and gastric cancer, can severely affect the quality of life, highlighting the need for effective diagnostics and treatments. Recent advances in minimally invasive technologies have led to wireless capsule endoscopes (WCEs), pill-sized devices with cameras and sensors that provide real-time imaging of the GI tract without sedation or traditional endoscopy.<sup>1</sup> WCEs have revolutionized GI diagnostics, especially in hard-to-reach areas. Advancing beyond passive imaging, gastric residency devices are engineered to remain in the GI tract for extended periods, enabling sustained monitoring, targeted therapy, or controlled drug release.<sup>2</sup> Featuring reconfigurable structures, responsive materials, and wireless communication, these devices offer a promising platform for personalized, long-term GI disease management.

However, powering these devices throughout their operational lifespan remains a significant challenge, especially during extended deployments. The power consumption of WCEs depends on the application, but most draw between 5 and 30 mW of power over a duration of 8–12 h, the majority of the power consumed by radiofrequency communications.<sup>3</sup> Thus, premature battery expiration affects roughly 16.5% of capsule endoscopy studies, while capsule retention occurs in roughly 1.3% of capsule endoscopies.<sup>1</sup> The risk of capsule retention increases with certain gastric conditions, such as obstructions within the GI tract.

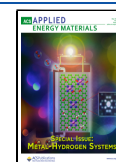
Furthermore, gastric residency devices typically consume less power than WCEs depending on the application (between 0.1 and 1 mW<sup>4</sup>) but require a long operating time (several days or weeks). As these devices become more advanced and

Received: February 14, 2025

Revised: April 28, 2025

Accepted: April 30, 2025

Published: May 13, 2025



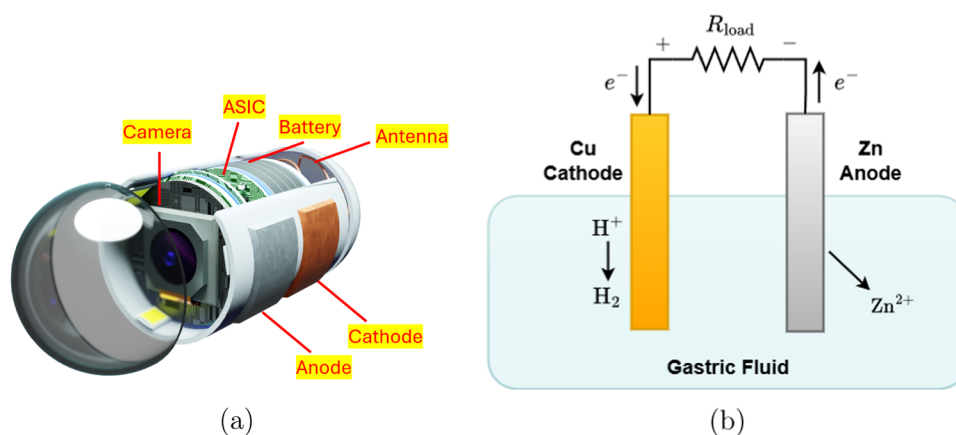
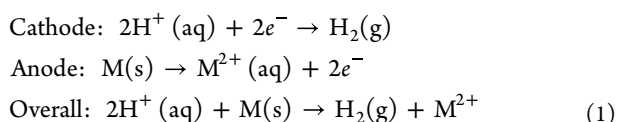


**Figure 1.** (a) Capsule endoscope model with a GI fluid-utilizing galvanic cell as a supplementary power source. (b) Schematic of a GI fluid-utilizing galvanic cell.

require greater power demand, energy harvesting techniques that provide a supplementary power source need to be investigated. Thus, energy harvesting methods, particularly galvanic cells utilizing GI fluid as an electrolyte in WCEs (Figure 1a) and gastric residency devices, present a promising solution. GI fluid-utilizing galvanic cells have been of interest as a supplemental power source owing to their biocompatibility, high energy capacities, and capabilities for extending longevity.<sup>5</sup> When these cells are placed in GI fluid, spontaneous reduction–oxidation reactions between the cathode and anode result in electric power generation. Figure 1b shows a schematic of a GI fluid-utilizing galvanic cell. The reactions of these galvanic cells (where M is an anodic metal such as Zn or Mg) are as follows:



Several publications have investigated the use of GI fluid-utilizing galvanic cells to power ingestible devices. The first galvanic cell for this purpose used gold (Au) and iron (Fe) as cathode and anode, respectively.<sup>6</sup> Since then, cathode–anode pairs such as platinum (Pt)-zinc (Zn),<sup>7</sup> palladium (Pd)-Zn,<sup>8</sup> Au-magnesium (Mg),<sup>9</sup> copper chloride (CuCl<sub>2</sub>)-Mg,<sup>10</sup> and magnesium chloride (MgCl<sub>2</sub>)-silver chloride (AgCl)<sup>11–13</sup> have been shown to generate enough power to perform certain tasks within the digestive tract. However, these studies are limited due to the small sizes of the devices or the very short-term intended uses (<1 h). Another study investigated circuitry for storing the harvested power and boosting the voltage of a galvanic cell (Pt–Mg) for use in ingestible devices.<sup>14</sup> A follow-up study used this combination to charge an ingestible thermometer that lasted 24 h.<sup>15</sup> However, the longevity and power characteristics of the Pt/Mg combinations were not reported. One study considered a setup with manganese oxide (MnO<sub>2</sub>) and activated carbon was considered as the cathode/anode pair, and it was found to generate a current in the range of 5 to 20 mA *in vitro* for 5 h.<sup>16</sup> Most relevant to this work is a study that performed long-term characterization of two pairs of electrodes, copper (Cu)-Zn and Cu–Mg.<sup>5</sup> The key findings most relevant to this work include the following:

- A 10 mm × 3 mm Mg anode generated power for 0.3 days, while a Zn anode generated power for 7 days in a pH 4 buffer solution.
- Cu–Mg had a cell voltage 1.3 times higher and a peak power density 6 times higher than Cu–Zn.
- Peak power generation was similar for varying sizes for both electrodes.
- The Cu–Zn combination was used to power a wireless endoscopic capsule in an *in vivo* porcine model for an average of 6.1 days over eight trials.
- Peak power generated was 100 times higher in the stomach than in the small intestine.

These results show promise for using galvanic cells to power devices in the gastric tract but demonstrate a need for systematic characterization of differing electrode pairs in different GI conditions. Furthermore, these results seem to account only for electrode performance for gastric residency devices due to the long-term nature of the study. As seen in the literature review, all of the previous studies only consider one or two electrode pairs and focus on either short-term or long-term applications. Currently, there is not an exhaustive characterization of the best-performing electrode pairs for both short- and long-term applications. Moreover, there is a lack of characterization of the performance of these cells when faced with differing gastrointestinal conditions, as well as if there is an effect on performance if the cathode size differs from the anode size. Thus, in this paper, we seek to systematically characterize the cell performance of a multitude of differing electrode combinations in varying conditions. The contributions of this paper can be summarized as follows:

- We present and analyze the results of *in vitro* power generation experiments involving six different cathode choices and three different anode choices in synthetic gastric fluid (SGF).
- We propose titanium (Ti), niobium (Nb), and molybdenum (Mo) as potential cost-effective, biocompatible cathode choices and compare them to the performance of Cu, Pt, and Pd. We also investigate the AZ31B Mg alloy as an anode and compare its performance to Zn and Mg.
- We assess the results of the different electrode combinations in terms of parameters such as longevity and energy capacity to determine their applicability to short-term or long-term applications.

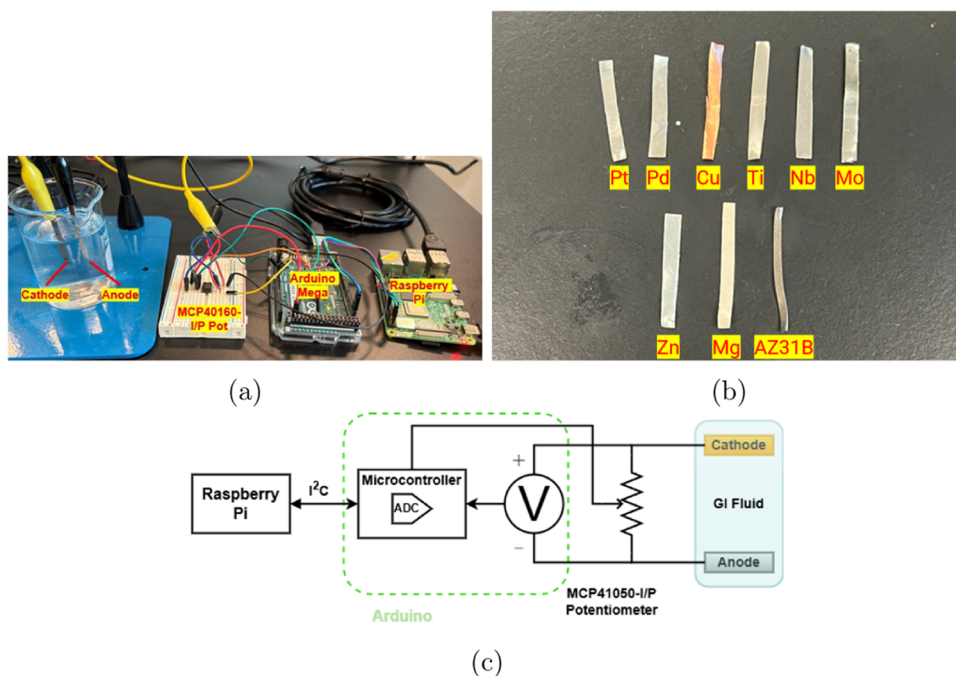


**Figure 2.** (a) Example experiment running to test the galvanic cell performance in SGF. (b) Electrodes are investigated in this paper. (c) Schematic of the experimental setup.

- We present the results of *in vitro* experiments to characterize the performance of short-term and long-term combinations in differing gastric conditions, such as varying gastric pH, stomach bleeding, etc., as well as the performance in the higher pH phosphate buffer solution (pH = 7.4) to represent intestinal fluid.
- We assess the effect of varying anode size with respect to cathode size on the effect of the cell performance.

The rest of the paper is organized as follows. **Section 2** discusses the overall experimental setup and materials used in this paper. **Section 3** introduces the selected cathodes and anodes and their characteristics, evaluates their performance in SGF, and discusses their applicability for short- or long-term applications. It also presents and evaluates the effect of simulated intestinal conditions, varying gastric conditions, and varying electrode sizes on cell performance. **Section 4** provides the summary, conclusions, and potential future impacts of this work.

## 2. EXPERIMENTAL SECTION

**2.1. Materials.** 37% hydrochloric acid, sodium chloride, pepsin, phosphate buffer solution, and the foils of zinc, magnesium, AZ31B, copper, titanium, niobium, platinum, palladium, and molybdenum were purchased from Sigma-Aldrich. Sugar and porcine blood were purchased at a local market in Atlanta.

**2.2. Synthesis of Synthetic Gastric Fluid.** SGF was prepared as described in a previous work.<sup>17</sup> To prepare SGF, 0.16 g of sodium chloride was added to 80 mL of deionized water, and then enough 37% hydrochloric acid was added so that the solution reached the desired pH (1.2 in the experiments without any gastric conditions). Finally, pepsin was added (0.256 g) before the experiments were to begin.

**2.3. Preparation of Electrodes.** All of the electrodes investigated in this paper were cut to have a volume of  $15 \times 3 \times 0.25 \text{ mm}^3$  in contact with the solution, except for the AZ31 Mg alloy and Mo. The AZ31 Mg alloy had twice the thickness compared to the other electrode materials and was thus cut to match their volume at  $15 \times$

$1.5 \times 0.5 \text{ mm}^3$ . Mo was also thicker but was cut at  $15 \times 3 \times 0.5 \text{ mm}^3$  to maintain a comparable surface area to the other cathodes.

**2.4. Measurement Setup.** The experimental setup comprises the cathode and anode electrodes, SGF solution or 1 M PBS, the MCP41050-I/P voltage-controlled digital potentiometer (Pot), Arduino Mega, and a Raspberry Pi (see **Figure 2a,c**). During the experiments, the cathode and anode were dipped into SGF or PBS and placed 1 cm apart to ensure that the Ohmic losses stemming from the distance between the electrodes were held constant. The electrodes were then connected to a digital potentiometer to characterize the electrochemical cell's performance. An Arduino Mega controls the digital potentiometer to perform a load-sweep from 50 k $\Omega$  to 150  $\Omega$  in 255 linear steps, each step lasting 2 s, followed by a 64-s hold at 50 k $\Omega$  to reset electrodes. Arduino ADC measures the load resistor voltage, while the Raspberry Pi records it via an I<sup>2</sup>C interface. The digital potentiometer has a maximum integral nonlinearity (INL) and differential nonlinearity (DNL) of  $\pm 1$  LSB, while the Arduino ADC has a maximum INL and DNL of  $\pm 0.5$  and  $\pm 0.25$  LSB, indicating minimal systematic error in the measurements. The experiments in this article are conducted at room temperature (25  $^{\circ}\text{C}$ ). However, a practical implementation would have the galvanic cell under human body temperature (37.5  $^{\circ}\text{C}$ ). At body temperature, the electrolyte conductivity and reaction kinetics would increase, but the cell voltage would decrease (according to the Nernst equation). Nonetheless, the effect of temperature on cell performance is independent of the effects of electrode choice, differing electrolyte conditions, and varying electrode size. Thus, the trends observed in this work likely remain the same. The experiments are conducted over several days to observe electrode performance over different load conditions over a long period of time. By performing these experiments and measuring the load voltages over time, we can characterize the performance of the galvanic cell in terms of parameters such as energy capacity, peak power rate, and longevity. MATLAB was used to compute the power generation rate  $P(t)$  over time using the measured voltage  $V(t)$  and load resistance  $R(t)$  with the simple equation

$$P(t) = \frac{V(t)^2}{R(t)} \quad (2)$$

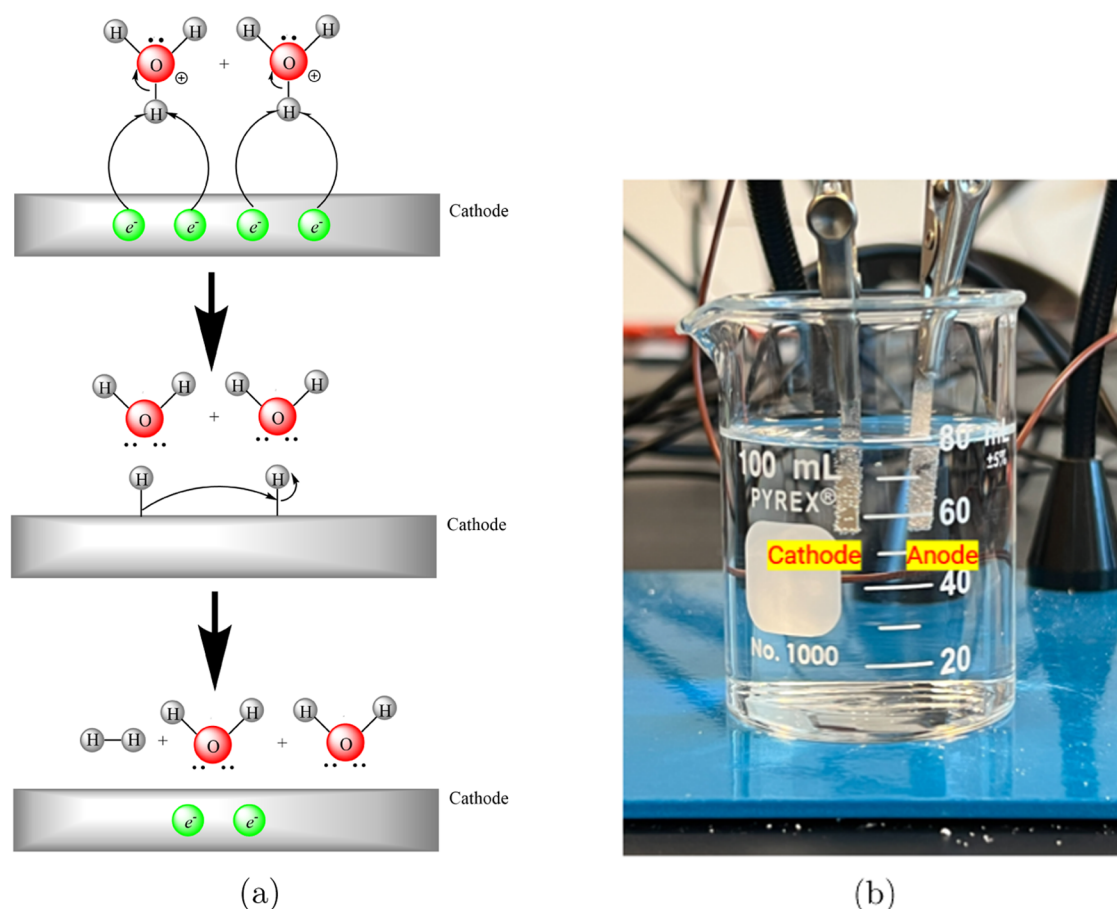


**Figure 3.** (a) Mechanism of H<sub>2</sub> evolution on the cathode. (b) Bubble formation on the cathode (Pt) due to the reduction reaction and the anode (Mg) due to the parasitic side reaction.

Then, the peak power over each load-sweep was computed, normalized over the dissolved anode volume (to account for any discrepancies in the sizes of the cut electrodes), and plotted over time. The energy capacity of each galvanic cell  $E$ , or the total power generated over the duration of the experiment  $\tau$ , was computed over the duration of the experiment as follows

$$E = \int_0^{\tau} P(t) dt \quad (3)$$

To account for any discrepancy in the sizes of the anodes (and potentially account for devices that require different electrode dimensions), the energy capacities were normalized over the anode volume by dividing the amount of mass dissolved of the anode  $m$  and multiplying by the density of the anode  $\rho$ , as shown in (4)

$$E_{\text{normalized}} = \frac{\int_0^{\tau} P(t) dt}{m} \rho \quad (4)$$

Finally, the maximum peak power of all load sweeps was measured and tabulated.

### 3. RESULTS AND DISCUSSION

**3.1. Characterization of Different Electrodes.** To characterize each cathode and anode's performances in SGF and determine the ideal combination for short-term and long-term applications, experiments were conducted for each cathode (Pt, Pd, Cu, Ti, Nb, and Mo) and anode (Zn, Mg, and AZ31B) pair, totaling 18 total experiments. The load-sweep setup was used, as described in Section 2, and the voltages of each cell over time were measured. MATLAB was

used to calculate and plot the normalized peak power over each load-sweep over time, as well as the voltage over time. The energy capacity of each cell was also computed and normalized over anode volume to account for any discrepancy in the sizes of the anodes. Finally, the longevity of each cell was measured. The parameters were then analyzed to determine the ideal cathode–anode pair for short-term and long-term ingestible device applications.

**3.1.1. Cathodes.** In this paper, Pt, Pd, Cu, Ti, Nb, and Mo are investigated as cathodes owing to their biocompatibility and ability to perform reduction reactions in gastric conditions. Pt, Pd, and Cu were investigated as cathodes for GI fluid-utilizing galvanic cells in several previous studies,<sup>5,7,8</sup> but their long-term performance has not been evaluated. Ti, Nb, and Mo have not been reported as cathodes in the literature but are identified in this paper as potential cathode choices due to their biocompatibility, low cost, and cathodic behavior in GI fluid.<sup>18–20</sup> Furthermore, Mo has been shown to be fully biodegradable, affording applications for transient electronics or devices that fully biodegrade after its operation.<sup>20</sup> In galvanic cells within GI fluid, cathode materials require reduction potentials exceeding hydrogens to favorably undergo the hydrogen evolution reaction (HER). Figure 3a illustrates the mechanism of the HER on the cathode. Despite a cathode material's standard reaction potential possibly being less than zero (such as in the case of Nb, Ti, or Mo), it may still function as a cathode due to differing dissolved salt or acid concentrations in GI fluid than standard conditions (298 K,

1 atm, and 1 M concentrations of each solute). This is illustrated by the following Nernst equation

$$U_{\text{cell}} = U_{\text{cell}}^{\theta} - \frac{RT}{nF} \ln(Q) \quad (5)$$

where  $U_{\text{cell}}$  is the reduction potential under the specific reaction conditions,  $U_{\text{cell}}^{\theta}$  is the standard reduction potential of the overall galvanic cell reaction,  $R$  is the ideal gas constant,  $T$  is the temperature,  $n$  is the number of electrons transferred per reaction,  $F$  is Faraday's constant, and  $Q$  is the reaction quotient, which is dependent on the concentration of the reactants and products (as well as the partial pressure of products in the gas phase, such as  $\text{H}_2$ ). Passivation, or a coating that a material may form when exposed to the environment, preventing it from further corrosion, may also result in an increase in the reduction potential, leading it to function as cathode. However, the oxide layer can reduce the number of active sites for the reduction reaction, thus potentially reducing the efficiency. In ambient conditions, Cu, Nb, and Ti passivate, so it is anticipated that passivation will reduce their performance as cathodes. The overall hydrogen evolution reaction is represented by the following chemical formula



The principal mechanism of the HER is based on three reactions.<sup>21</sup> The first is Volmer's reaction, where a hydrogen ion is adsorbed from the cationic hydronium present in the acidic solution onto the metal surface as follows



The adsorbed hydrogen atom can then participate in two other reactions where hydrogen gas is formed. In Tafel's reaction, two adsorbed hydrogens recombine to form hydrogen gas.



In Heyrovsky's reaction, the electrochemical desorption of the adsorbed hydrogen occurs to form hydrogen gas.



As the stability of transition states depends on the cathode material chosen,<sup>22</sup> the amount of energy required to complete this process depends on the cathode material. According to the results, the choice of cathode clearly plays a role in the peak power generation rate and energy capacity when the anode remains the same. The cathodes rank in terms of normalized energy capacity and peak power as follows

$$\text{Pt} \approx \text{Pd} > \text{Mo} > \text{Cu} > \text{Ti} \approx \text{Nb} \quad (10)$$

This correlates with the hydrogen activation overpotential of each material, which quantifies a material's ability to perform the HER. The magnitude of the HER activation overpotential for a material is largely determined by its electronic structure and catalytic activity. Of all pure metals, Pt-group noble metals such as Pt and Pd typically exhibit hydrogen binding energy closest to optimal, where hydrogen is neither too strongly nor too weakly adsorbed. If hydrogen is too strongly adsorbed, the reactive site is blocked, preventing reaction, while if hydrogen is weakly adsorbed, the transition state is unstable and the reaction fails to occur.<sup>22</sup> This principle is reflected in each material's activation overpotential. Of the cathodes chosen in this study, Pd and Pt exhibit the lowest activation overpotentials for the HER, Mo and Cu are in the midrange, and Ti

and Nb have the highest overpotentials (see Table 1).<sup>23</sup> Interestingly, Pt outperforms Pd in terms of energy capacity in

**Table 1. Comparison of Different Cathodes**

material	Cu	Pd	Pt	Nb	Ti	Mo
hydrogen activation overpotential	mod.	low	low	high	high	low–mod.
standard reduction potential (V)	0.337	0.915	1.188	−1.099	−1.63	−0.2

the cases when Zn and Mg are anodes but slightly underperforms when the AZ31 alloy is the anode. Pt and Pd have similar hydrogen activation overpotentials (−0.09 V at 22.5 °C),<sup>23</sup> so the small variance between the results of Pt and Pd is likely negligible. In Table 3, Pt and Pd comparatively achieved the highest energy capacities and peak powers. This can be attributed to their noble and catalytic activity. Next, Mo appears to underperform Pt and Pd but outperforms Cu significantly. Finally, Cu outperforms Ti and Nb. The longevity of the galvanic cell appears to vary on the choice of the cathode, but the rankings of longevity for each cathode when the anode remained the same were inconsistent. For example, the longevity of the Cu–Zn combination was less than that of most other cathode–Zn combinations, but the longevity of the Cu–AZ31 combination was greater. There are likely other factors that affect the longevity aside from cathode selection, such as the choice of anode.

Since Pt and Pd exhibit the best energy capacity and peak powering rate over time, Pt and Pd are the ideal selections for cathodes in future applications when opting for superior energy harvesting capabilities. However, as Pt and Pd are relatively expensive, Mo may also be an optimal cathode choice for devices when cost is a factor. Over recent years, Mo has also shown promise for biodegradable electronic systems that can dissolve without a trace after their function within the body.<sup>20</sup> Thus, Mo could potentially also be an ideal cathode selection for a cell used to power fully transient ingestible devices.

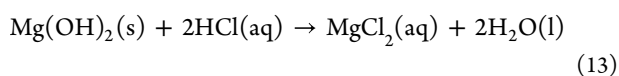
**3.1.2. Anodes.** Zn, Mg, and the AZ31B Mg alloy are chosen as anodes owing to their biocompatibility, dietary value when dissolved, high specific energy capacities, and highly negative reduction potentials favoring the electrochemical reaction. The Zn and Mg cations produced by the anodic reaction are well-known for their role in the body as trace nutrients, and the rate the ions are produced has been shown to be well below the US Food and Nutrition Board upper limit.<sup>5</sup> Zn and Mg have also been investigated in prior works for GI fluid-utilizing galvanic cells, but their performance has not been fully characterized.<sup>5,7,9</sup> The AZ31 alloy has not been investigated in prior works, but its alloyed components (Mg and other trace elements) are fully biocompatible at the rate that the anode degrades.<sup>23</sup> During these experiments, we also attempted to test Nb and Ti as anodes, as their specific reduction potential is less than 0 V. However, Ti and Nb generated little to no voltage as anodes and instead functioned as cathodes in the simulated gastric conditions. An example oxidation reaction taking place at an anode (Zn) for a GI fluid-utilizing galvanic cell is as follows



At the anode, material oxidation provides electrons for circuit flow, impacting cell performance. Thus, the performance of the cell is also contingent on the anode material. Material densities, specific current capacities, and half-reaction reduction potentials may determine the total current supplied to the ingestible device and the cell potential, affecting both the power supply and anode reaction rates, thus potentially influencing cell longevity. While Mg theoretically surpasses Zn in power capabilities due to higher specific capacity and reduction potential,<sup>24</sup> it undergoes an unfavorable side reaction in aqueous solutions, which competes with the favorable electrochemical reaction. Previous works have suggested that this phenomenon hinders the performance of the galvanic cell when Mg is the anode.<sup>5,10</sup> The side reaction is as follows



In an acidic solution (such as SGF), the solid  $\text{Mg(OH)}_2$  then reacts with the acid in a neutralization reaction



To account for this, the performance of the Mg alloy AZ31 (Mg96–Al3–Zn1) is also investigated as an anode. Its alloying of Al and Zn affords corrosion resistance through the formation of protective oxide layers while maintaining biocompatibility.<sup>25</sup> Thus, the oxide layer should interfere with the parasitic side reaction of Mg. Due to this, it is anticipated that the AZ31 Mg alloy could perform better as an anode than pure Mg.

In these experiments, Mg was observed to have a superior peak powering rate compared to AZ31 and Zn when cathodes with lower activation overpotentials (Mo, Pt, and Pd) were used. However, AZ31 outperformed (or performed similarly to) Mg and Zn when the high hydrogen activation overpotential cathodes (Cu, Ti, and Nb) were used (see Table 3). AZ31 has increased corrosion resistance due to its alloying elements, which produce protective oxide layers (passivation). These layers provide protection against Mg's parasitic side reaction and can also reduce the kinetics of the favorable electrochemical reaction. Pure Mg, lacking these protective elements, corrodes more rapidly and is more susceptible to side reactions. As such, when cathodes with low activation overpotentials are used, the kinetics of the HER will significantly outweigh that of the side reaction, causing pure Mg to outperform more corrosion-resistant AZ31. Conversely, when materials with high activation overpotentials are used, the kinetics of the HER becomes closer to that of the parasitic side reaction. As AZ31 more readily resists the side reaction, it generates a higher powering rate in comparison to pure Mg in this case. Regardless of cathode selection, both AZ31 and pure Mg exhibit significantly higher powering rates than Zn, due to Mg's significantly higher reduction potential (see Tables 2 and 3).

**Table 2. Comparison of Different Anodes**

material	Zn	Mg
standard reduction potential (V)	−0.76	−2.36
specific capacity (mAh g <sup>−1</sup> )	819.87	2205.42
density (g cm <sup>−3</sup> , 25 °C)	7.14	1.738
side reaction	no	yes

**Table 3. Energy Parameters of Cathode–Anode Combinations**

combination	norm. peak power	energy capacity	norm. energy capacity	lifetime
	( $\mu\text{W mm}^{-3}$ )	(mWh)	( $\mu\text{Wh mm}^{-3}$ )	
Cu–Zn	3.84	1.29	123.42	4.85
Nb–Zn	0.94	0.77	54.26	4.85
Ti–Zn	2.62	1.18	88.48	5.19
Pd–Zn	72.66	9.95	914.30	6.12
Pt–Zn	101.34	11.27	1260.66	7.08
Mo–Zn	21.99	3.21	281.25	5.97
Cu–Mg	127.12	0.47	38.09	0.22
Nb–Mg	55.99	0.45	25.74	0.25
Ti–Mg	51.65	0.53	32.75	0.31
Pd–Mg	823.69	1.09	101.05	0.12
Pt–Mg	880.66	1.19	105.21	0.10
Mo–Mg	211.13	1.10	77.75	0.367
Cu–AZ31	121.48	8.44	604.34	5.06
Nb–AZ31	103.66	3.94	406.83	3.02
Ti–AZ31	84.40	3.83	386.73	3.21
Pd–AZ31	388.44	13.99	1184.82	4.48
Pt–AZ31	402.18	9.449	1062.58	3.98
Mo–AZ31	232.46	8.225	805.69	4.86

Despite Mg's superior energy generation rate for the ideal cathodes with lower hydrogen activation overpotential, Mg's susceptibility to the side reaction, as well as its higher reduction potential and thus reaction kinetics, inhibits the galvanic cell's energy capacity and lifetime. Theoretically, Mg's higher specific capacity should afford a higher energy capacity than Zn, but each cathode–Mg combination underperformed each respective cathode–Zn combination in that regard, likely due to the unfavorable side reaction of Mg. However, the AZ31 alloy appears to exhibit comparable or superior energy capacities than Zn and comparable or slightly lower lifetimes, owing to its corrosion resistance and stability (Table 3).

For the cases with Zn and AZ31 as the anode, the power plots (Figure 4a,d) are characterized by an initial steep hike in power generation when the electrodes contact the solution, which slowly dissipates over a few minutes (Figure 4b). This phenomenon is explained by the 'bubble overpotential', as the formation of hydrogen gas bubbles on the cathode results in a lesser surface area for hydrogen to be reduced (see Figure 3b). After a few hours of electrode contact with the electrolyte, the power slowly increases until it reaches a steady state. This occurrence is explained by the presence of Zn and AZ31's protective oxide surface coating formed by passivation before contact with the solution. Over the few hours after contact, the oxide coating began to dissolve, exposing the surface area of the pure metal to the electrolyte. Exposure of the surface area of the pure metal leads to an increase in the power generation rate, as well. Furthermore, as the Zn/AZ31 dissolves, its surface area decreases, resulting in a small but noticeable decrease in power generation over time (see Figure 4b). The plot (see Figure 4c) of the Mg combinations is characterized by a short stabilization (1 h) followed by a quick but gradual decrease as the Mg anode dissolves rapidly due to the low reduction potential and side reaction.

Supplementary tests were performed to determine the internal resistance of the Pt–Zn, Pt–Mg, and Pt–AZ31 combinations (Supporting Information Table S4). Pt was chosen due to its optimal performance as a cathode, as

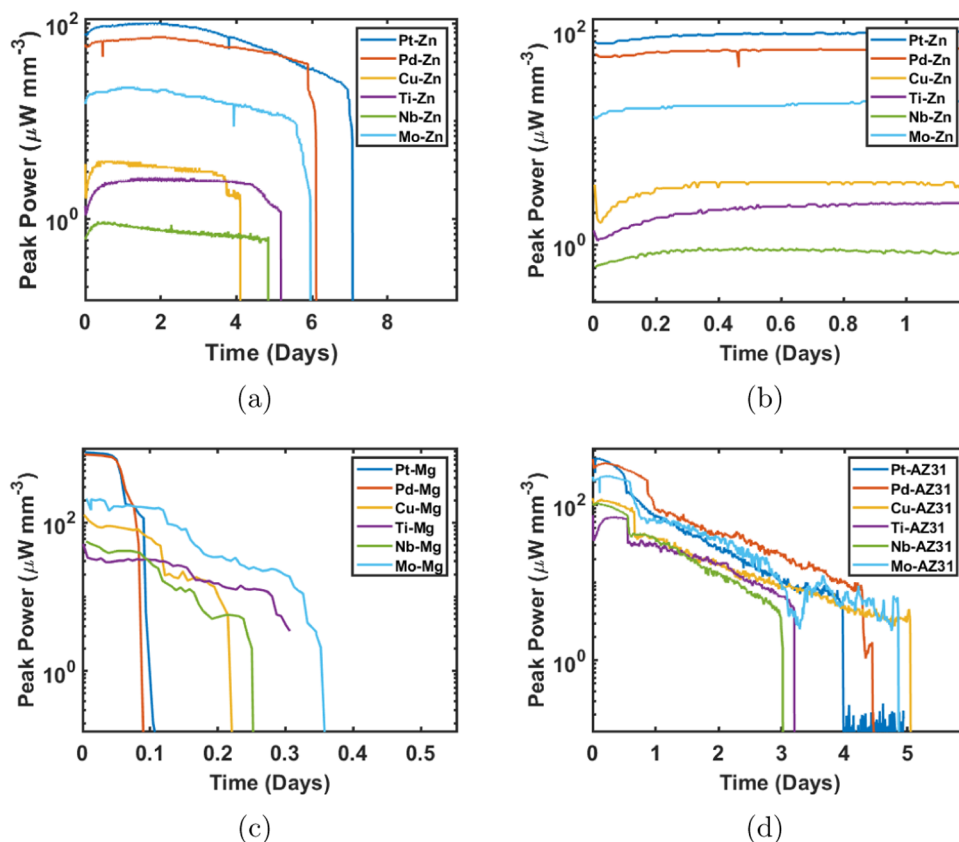


**Figure 4.** Peak power for each load-sweep over time under SGF conditions for different cathode–anode combinations: (a) cathode–Zn combinations, (b) cathode–Zn combinations for the first 1.2 days, (c) cathode–Mg combinations, and (d) cathode–AZ31 combinations.

discussed in Section 3.1.1. Pt–Mg was observed to have the lowest internal resistance, followed by Pt–AZ31, then Pt–Zn. Tests were also performed to characterize these combinations under set load resistances of 47  $\Omega$ , 150  $\Omega$ , 247  $\Omega$ , 1 k $\Omega$ , and 10 k $\Omega$  (see Supporting Information Section Figure S2 and Tables S5–S7). Pt–Zn and Pt–AZ31 had the highest energy capacities at their internal resistance values, but Pt–Mg had its highest energy capacity under a load of 10 k $\Omega$ , suggesting that a higher load resistance may stabilize the Mg anode from the side reaction.

As the properties of the anodes vary vastly, the optimal anode selection depends on the application. Thus, for short-term devices, which only remain in the gastric environment for a maximum of 4 h, Mg may be the superior choice of anode, as the power generation rate of these cells drops significantly after entering the intestinal tract.<sup>5</sup> Over this short period, Mg would easily generate the most power when paired with an appropriate cathode. In this case, energy storage mechanisms would need to be employed to allow the energy harvested to supplement the device's power requirements within the intestinal tract. However, the Pt–Mg and Pd–Mg pairings generate roughly 8–10 mW at their peak power, which is sufficient enough to power many WCEs.<sup>3</sup> For long-term devices, i.e., resident in the gastric environment for a long period, AZ31 and Zn are more suitable choices, as they experience superior longevity while maintaining a consistent powering rate. Importantly, the peak power rate when Pt and Pd were the cathode with these anodes could potentially be high enough to power gastric residency devices alone.<sup>4</sup> Nonetheless, if a long-term device requires immediate powering needs or a higher energy demand over time, AZ31

is a more optimal choice. However, if the device requires a higher battery longevity, then Zn may be a better choice.

**3.2. Evaluation of Electrode Performance in Various GI Conditions.** **3.2.1. Influence of Differing pH Values.** The experiments done in Section 3.1 are performed under a pH of 1.2, which corresponds to the pH when the stomach is in the 'fasted-state', or the postabsorptive state when any food or drink has been fully digested. This pH value is suitable for simulating the conditions undergone by WCEs since their usage requires their patients to be in a fasted state. However, the effect of different pH values becomes crucial in the cases of long-term devices and the presence of GI disorders. Even in the absence of GI disorders, the pH of gastric fluid fluctuates over time due to food intake and the regulation of acid secretion, with values typically ranging from 1 to 3. These fluctuations have been shown to differ between men and women, as well as by different age groups.<sup>26</sup> Moreover, conditions such as bile reflux, *H. pylori* bacterial infection, chronic inflammation, gastric ulcers, and cancer have been shown to cause hypoacidity or reduced acid concentration in the gastric tract.<sup>27</sup> Since the hydrogen ions are participants of the cell reaction, changes in pH, and thus hydrogen ion concentration, can affect the cell performance.

Therefore, a similar experimental setup as described in Section 2 is undertaken to investigate the effect of pH on cell performance. For these experiments, AZ31B is chosen as the anode and Pt is chosen as the cathode. For the electrolyte, SGF is synthesized as described previously, but varying amounts of HCl are added to the solution to test different pH values. pH values of 2 and 3 are tested alongside the pH of 1.2 as a control, and the results are compared to the results of the pH

1.2 or fasted-state experiment. Each experiment is run for 2.7 days to ensure that the results are not affected by growth in the moist SGF environment.

Overall, the results show that the performance of the GI fluid-utilizing galvanic cell is significantly affected by pH. As pH increases from 1.2 to 3, the normalized power generation rate, normalized peak power, and total energy generated over the duration of the experiments decrease. As the pH increases, the concentration of protons available to participate in the cathode half-reaction decreases exponentially. In accordance with chemical reaction kinetics, this fact thus decreases the rate at which the galvanic cell reactions can occur and thus contributes to the lowered energy parameters as pH increases from 1 to 3. However, as the pH increased from 3 to 4, the energy generated over 2.7 days increased. In the plots, the rate at which the peak power generation rate over time decreased correlated with decreasing pH. Thus, at roughly 1.7 days, the power generation rate of the pH 4 case exceeded all other cases, as it remained much more consistent over time. The less harsh corrosive conditions of a higher pH electrolyte could result in a more consistent power plot, potentially explaining why the raw energy capacity of the pH 4 case exceeded that of the pH 3 and the normalized energy capacity of the pH 4 case exceeded all others. The energy capacity is negatively affected by losing energy to the side reaction; therefore, reduced kinetics of the side reaction may improve the overall energy efficiency of the galvanic cell.

Even though the energy generation rate drops tremendously with the increase in pH, the normalized total energy generated increases as the pH increases. In the pH 1.2 case, the entirety of the anode contacting the solution (20.48 mg) dissolved within 2.9 days. However, in the pH 2 case, pH 3 case, and pH 4 case, only 5, 2.21, and 2.42 mg dissolved during the aforementioned duration, respectively. As the pH of the solution increases (at least from 1.2 to 4), the corrosive environment becomes much less aggressive toward the galvanic cell and limits the parasitic side reaction at the anode, affording a greater energy efficiency.

As expected, when the pH increases and the galvanic reaction rate decreases, the longevity of the galvanic cell should increase as well. We observed this phenomenon for the pH 2 case, with it lasting over 7 days (see Supporting Information Table S8 and Figure S4). Interestingly, the normalized energy capacity for the pH 2 case greatly exceeded the pH 1.2 case. However, the longevity of the pH 3 case could not be measured in this way, as the stagnant, higher pH SGF can attract mold, which not only induces contamination but also results in a significant pH increase over time, which affects the results.

Even though only one combination (Pt–AZ31) was tested under the varying pH conditions, the trends observed in these results should be expected for other electrode combinations; as pH increases, the longevity and normalized energy capacity should increase, while the energy generation rate should decrease. The effect of the electrode properties on the performance is independent of the effect of the solution.

Table 4 shows the computed energy parameters where the Pt–AZ31 combination is placed in SGF of differing pH, and Figure 5a shows the peak power plot for this case.

**3.2.2. Influence of Differing Electrolyte Concentration.** In addition to acidity, factors such as dietary intake and metabolic activity throughout the day also affect the concentrations of electrolytes such as  $\text{Na}^+$ ,  $\text{K}^+$ , and  $\text{Cl}^-$  in the stomach.

**Table 4. Energy Parameters of the Pt–AZ31 Combination in Differing pH Solutions**

combination	peak power ( $\mu\text{W}$ )	norm. peak power ( $\mu\text{W mm}^{-3}$ )	energy generated over 2.7 days (mWh)	norm. energy capacity over 2.7 days ( $\mu\text{Wh mm}^{-3}$ )
pH 1.2	5486.0	472.49	10.666	918.80
pH 2	977.75	349.31	4.712	1683.5
pH 3	244.44	196.08	2.585	2074.0
pH 4	213.43	159.00	3.349	2494.8

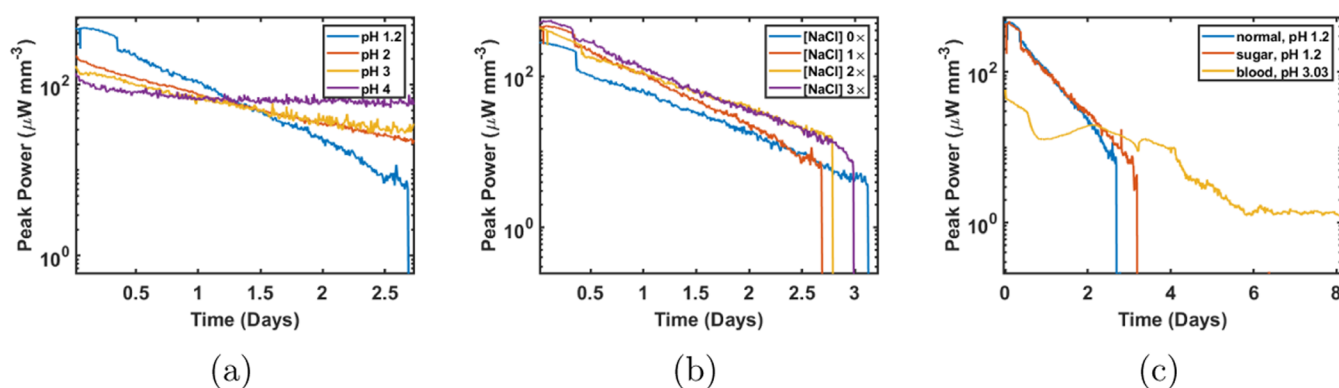
Furthermore, the presence of gastric diseases and disorders is also known to affect electrolyte concentration.<sup>28</sup> Even though  $\text{H}_3\text{O}^+$  is the major electrolyte in the stomach that participates in the cell reaction, nonparticipating ions in the stomach can affect cell performance. The concentration of dissolved ions directly correlates with the conductivity of the electrolyte. In an electrochemical cell, an amount of potential is lost on the way (thus, an overpotential) as current flows through the electrolyte, known as an Ohmic drop. As the conductivity of the electrolyte increases, the resistance decreases, resulting in a smaller Ohmic drop. Thus, an increase in electrolyte conductivity will likely increase the performance of these galvanic cells. To determine the effect of differing electrolyte concentration, the experimental setup described in Section 2 is performed with two experiments doubling and tripling the NaCl concentration, respectively, and one experiment removing the NaCl altogether. Pt and AZ31 are used as the cathode and anode, respectively.

Table 5 shows the computed energy parameters from the experiments where the Pt–AZ31 combination is placed in SGF of differing NaCl concentrations, and Figure 5b shows the peak power plot for this case.

Increasing the concentration of NaCl results in a higher normalized energy capacity, normalized peak power, and normalized energy generation rate over time. As the dissolved salt concentration increases, the solution's ionic mobility and conductivity increase, which lowers the internal resistance of the galvanic cell and allows more power delivery. However, this effect is less pronounced compared to the impact of varying pH levels, except when no other salts are present besides the acid (as the absence of salts drastically decreases the conductivity of the solution). The impact of varying salt concentrations on cell longevity is inconclusive but likely negligible since the pH and anode choice remained constant throughout the experiments.

**3.2.3. Effect of Foreign Substances.** With the previous two sections in mind, the presence of foreign substances in the gastric fluid, such as blood (due to bleeding) or food, may also have an effect on cell performance. These foreign substances can impact the acidity and electrolyte concentration, as detailed previously. Furthermore, larger particles may obstruct the reactive sites of the electrodes, potentially hindering the cell performance. Finally, foreign substances may also contain reducing or oxidizing agents of their own and thus participate in the galvanic reaction.

A similar experimental setup, as found in Section 2, is repeated with SGF, but with the addition of several foreign substances to the SGF. The first experiment involves the addition of 1 g of table sugar (sucrose). The second experiment involves 1/4 of the SGF (20 mL) being replaced with porcine blood. The third experiment involves food being



**Figure 5.** Peak power for each load-sweep over time for galvanic cells under (a) differing pH values, (b) differing NaCl concentrations, and (c) SGF with different foreign substances.

**Table 5. Energy Parameters for the Pt–AZ31 Combination under Differing NaCl Concentrations**

combination	norm. peak power ( $\mu\text{W mm}^{-3}$ )	energy capacity (mWh)	norm. energy capacity ( $\mu\text{Wh mm}^{-3}$ )	lifetime (days)
[NaCl] 0x	423.66	7.873	614.66	3.12
[NaCl] 1x	472.49	10.67	919.14	2.69
[NaCl] 2x	509.20	10.13	981.98	2.79
[NaCl] 3x	555.23	12.95	1101.5	2.98

inserted into the SGF. The pH of each solution after the addition of each foreign substance is measured and recorded before the experiment. Pt and Mg are used as the cathode and anode, respectively.

Table 6 shows the computed energy parameters from the experiments where the Pt–AZ31 combination under SGF with

**Table 6. Energy Parameters for the Pt–AZ31 Combination with SGF and Differing Added Substances**

combination	norm. peak power ( $\mu\text{W mm}^{-3}$ )	energy capacity (mWh)	norm. energy capacity ( $\mu\text{Wh mm}^{-3}$ )	lifetime (days)
normal	472.49	10.67	919.14	2.69
sugar added	473.78	11.25	931.46	3.19
blood added	279.88	8.56	513.89	12.44

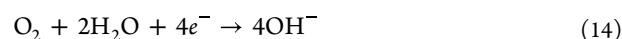
different added substances, and Figure 5c shows the peak power plot for this case.

The addition of sugar appears to not produce any significant difference, as the normalized energy capacity for the addition of sugar and the case where no extra substances were close, while the peak power and longevity were similar. The overall power generation rate looks to be higher in the sugar case than in the normal case, but this could also be explained by the fact that the anode size was slightly larger in that case. Sucrose does not form ions in the solution and thus does not affect the conductivity of the solution. Thus, simple sugars likely do not participate in any capacity in galvanic cell reactions.

The introduction of blood to the SGF increased the pH to 3.03. Due to this, the power generation rate over time decreased while the longevity increased substantially. Interestingly, the energy capacity when blood was added significantly dropped compared with the case where pure SGF at pH 3 was used. After the experiment was completed, the cathode was observed to be coated with substances from the blood,

potentially indicating the adsorption and coating of solid materials to the electrode surface that interferes with the reaction and inhibits its efficiency. The observed adsorption of unwanted materials to the electrode surface could pose a major problem in true *in vivo* applications, especially in long-term gastric residency devices. Thus, future works using galvanic cells as a supplementary energy source should take proper care to shield the electrodes from the environment while allowing the desired substances (protons) to come into contact by using coatings such as Nafion, documented in works such as ref 8.

**3.2.4. Performance Inside Intestinal Fluid.** Endoscopic capsules generally pass through the stomach to the small intestine within 2 to 5 h. Thus, since a capsule using a galvanic energy harvester will likely enter the intestinal tract, an investigation into the harvester's performance in this fluid is also pertinent. Intestinal fluid (IF) has a widely different composition than gastric fluid, with its drastically lower pH (5.7 to 7.4) and differing salt concentrations. Indeed, a previous study found that the peak power generation rate of cells in intestinal fluid was 100 times less than in gastric fluid.<sup>5</sup> As the IF is much less acidic than gastric fluid, the dominating half-reaction at the cathode is instead:



In addition to the peak power generation rate in IF, the effect of IF on cell longevity and total energy capacity is investigated by performing the experimental procedure described in Section 2 in PBS to represent the IF. Pt is used as the cathode, and Mg is used as the anode. Table 7 shows the computed energy

**Table 7. Energy Parameters for the Pt–AZ31 Combination in SGF vs PBS**

combination	norm. peak power ( $\mu\text{W mm}^{-3}$ )	energy capacity (mWh)	norm. energy capacity ( $\mu\text{Wh mm}^{-3}$ )	lifetime (days)
SGF	472.49	10.67	919.14	2.69
PBS	109.81	8.944	931.23	> 8

parameters from the trial in which the Pt–AZ31 is under PBS, and Figure 6a shows the peak power plot for this case. In both the table and the plot, the results of the experiment under PBS are compared to the experiment under SGF.

In the pH 7.4 PBS, the normalized energy generation rate and normalized peak power of the galvanic cell appear to decrease compared to the pH 1.2 SGF, while the longevity

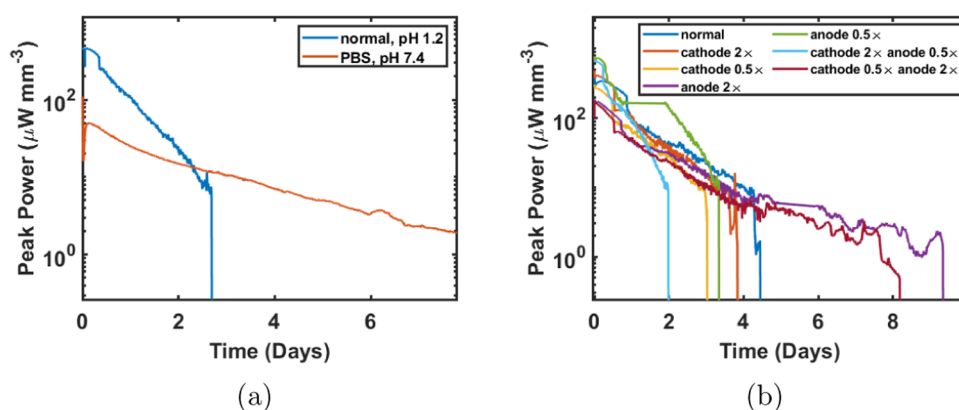


**Figure 6.** Peak power for each load-sweep over time for the galvanic cell under (a) PBS/simulated intestinal fluid and (b) SGF with varying electrode size combinations.

increases significantly. The results follow the trend of the previous results of differing pH values; the pH increase correlates with a decreased energy generation rate. However, the normalized energy capacity for the PBS case appears to match that of the pH 1.2 SGF instead of the expected increase with a pH increase. It is likely that the dominating reduction reaction described in Section 3.2.1 for higher pH values occurs at a very slow rate compared to that of the parasitic side reaction, limiting the efficiency of the galvanic cell at this pH.

**3.3. Varying Cathode and Anode Size Ratio.** In galvanic cell design for ingestible devices, the effect of varying the size ratio between the cathode and the anode has been unexplored. In a typical galvanic cell, the larger the cathode is with respect to the anode, the more reduction can occur, and thus, a greater current can be achieved.<sup>29</sup> However, this phenomenon has not been investigated for GI fluid-utilizing galvanic cells. To examine this phenomenon, we test four scenarios and compare them to the results in Section 3.1:

- Cathode size of  $15 \times 1.5 \times 0.25 \text{ mm}^3$  (cathode volume halved), anode size remains the same.
- Cathode size of  $15 \times 6 \times 0.25 \text{ mm}^3$  (cathode volume doubled), anode size remains the same.
- Anode size of  $15 \times 1.5 \times 0.25 \text{ mm}^3$  (anode volume halved), cathode size remains the same.
- Anode size of  $15 \times 6 \times 0.25 \text{ mm}^3$  (anode volume doubled), cathode size remains the same.

In this section, Pd is used as the cathode, and Mg is used as the anode. The same general experimental procedure is used as in Section 2 with SGF.

Table 8 shows the computed energy parameters from the trials where the cathode/anode size is changed with respect to the other anode, and Figure 6b shows the peak power plot for these cases. In both the table and the plot, the results of the experiments are compared to the experiment where the cathode-to-anode size ratio is the same. According to the results, as the ratio between the cathode size and the anode size increases, the normalized peak power and normalized energy generation rate increase. Increasing the surface area of the cathode allows more hydrogen ions to be reduced simultaneously, improving the overall reaction rate and decreasing the internal resistance of the galvanic cell.<sup>29</sup> Furthermore, as the anode surface area decreases, the amount of active sites for the side reaction to occur is decreased as well, allowing the favorable galvanic cell reaction to better dominate the side reaction. However, increasing the anode's dimensions

**Table 8. Energy Parameters for Differing Sizes of the Pd–AZ31 Combination**

combination	norm. peak power ( $\mu\text{W mm}^{-3}$ )	energy capacity (mWh)	norm. energy capacity ( $\mu\text{Wh mm}^{-3}$ )	lifetime (days)
Pd–AZ31	388.44	13.99	1184.82	4.48
cathode 2×	480.37	10.843	1084.3	3.84
cathode 0.5×	303.07	7.032	703.23	3.03
anode 2×	186.26	16.741	704.35	9.36
anode 0.5×	773.59	21.06	2970.21	3.34
cathode 2×, anode 0.5×	676.00	6.28	947.67	1.99
cathode 0.5×, anode 2×	174.60	13.43	703.26	8.18

affords greater cell longevity. The greater the volume of the anode, the more metal that can be reduced overall. Therefore, when considering the dimensions of galvanic cells for ingestible devices, one must choose a suitable cathode-to-anode size ratio that sufficiently generates enough power over time while ensuring that the anode is large enough to last the expected battery duration.

#### 4. CONCLUSIONS

In this work, the use of galvanic cells as a supplemental power source for ingestible devices was systematically characterized *in vitro*. Eighteen total experiments with six different cathodes and three different anodes were performed in synthetic gastric fluid, and the peak power generation over time, total energy capacities, and longevities were measured for each cathode–anode pair. It was observed that Pt and Pd are the superior choices in cathodes due to their low hydrogen reduction potential, but Mo is also a viable choice when considering affordability and transient electronics applications. Mg is the most suitable choice of the anode in short-term gastric devices, while the anode choice in long-term gastric residency devices depends on the application, with Zn or the AZ31B alloy being the optimal choice.

Moreover, the effects of differing gastric conditions on galvanic cell performance, as well as differing galvanic cell dimensions, were also investigated. The energy generation rate decreases with an increase in pH, but the power efficiency usually increases. As the dissolved salt concentration increases, the performance also increases. Large substances inside the gastric fluid can inhibit the electrodes from performing

efficiently. The energy generation rate in intestinal fluids rapidly drops compared to SGF and is overall less efficient. Finally, an increased cathode-to-anode size ratio greatly increases the powering efficiency, but larger anodes afford greater longevities.

The results of the experiments provide key insight into the effects of electrode choice, differing GI conditions, and differing galvanic cell dimensions for powering gastric devices. The conclusions in this paper will inform future work on the optimal galvanic cell design for providing supplementary power to ingestible devices.

## ■ ASSOCIATED CONTENT

### SI Supporting Information

The Supporting Information is available free of charge at <https://pubs.acs.org/doi/10.1021/acsaem.5c00463>.

Experiments and results for the measurement of voltage at the peak power, internal resistance, set load resistance, and pH 2 case, alongside an example characterization of the load-sweep setup (PDF)

## ■ AUTHOR INFORMATION

### Corresponding Author

Camden Kitchen – School of Electrical and Computer Engineering, Georgia Institute of Technology, Atlanta, Georgia 30332, United States; [orcid.org/0009-0007-4379-5017](https://orcid.org/0009-0007-4379-5017); Email: [ckitchen6@gatech.edu](mailto:ckitchen6@gatech.edu)

### Authors

Volkan Erturk – IHP GmbH - Leibniz Institute for High Performance Microelectronics, Frankfurt (Oder) 15236, Germany

Linhardt Ordella – School of Electrical and Computer Engineering, Georgia Institute of Technology, Atlanta, Georgia 30332, United States

Abhishek Swaminathan – School of Biomedical Engineering, Georgia Institute of Technology, Atlanta, Georgia 30332, United States

Seun Sangodoyin – School of Electrical and Computer Engineering, Georgia Institute of Technology, Atlanta, Georgia 30332, United States

Complete contact information is available at: <https://pubs.acs.org/doi/10.1021/acsaem.5c00463>

### Notes

The authors declare no competing financial interest.

## ■ REFERENCES

- (1) Robertson, K. D.; Singh, R. *Capsule Endoscopy*; StatPearls Publishing, 2023.
- (2) Mau, M. M.; Sarker, S.; Terry, B. S. Ingestible devices for long-term gastrointestinal residency: A review. *Prog. Biomed Eng. (Bristol)* **2021**, *3*, No. 042001.
- (3) Basar, M. R.; Malek, F.; Juni, K. M.; Idris, M. S.; Saleh, M. I. M. Ingestible wireless capsule technology: A review of development and future indication. *Int. J. Antennas Propag* **2012**, *2012*, No. 807165.
- (4) Yang, S.-Y.; Sencadas, V.; You, S. S.; Jia, N. Z.-X.; Srinivasan, S. S.; Huang, H.-W.; Ahmed, A. E.; Liang, J. Y.; Traverso, G. Powering implantable and ingestible electronics. *Adv. Func. Mater.* **2021**, *31*, No. 2009289.
- (5) Nadeau, P.; El-Damak, D.; Glettig, D.; Kong, Y. L.; Mo, S.; Cleveland, C.; Booth, L.; Roxhed, N.; Langer, R.; Chandrakasan, A.

P.; et al. Prolonged energy harvesting for ingestible devices. *Nat. Biomed Eng.* **2017**, *1*, No. 0022.

(6) Mackay, R. S.; Jacobson, B. Endoradiosonde. *Nature* **1957**, *179*, 1239–1240.

(7) Jimbo, H.; Miki, N. Gastric-fluid-utilizing micro battery for micro medical devices. *Sens Actuators B Chem.* **2008**, *134*, 219–224.

(8) Mostafalu, P.; Sonkusale, S. Flexible and transparent gastric battery: Energy harvesting from gastric acid for endoscopy application. *Biosens Bioelectron* **2014**, *54*, 292–296.

(9) Yoshida, S.; Miyaguchi, H.; Nakamura, T. Development of tablet-shaped ingestible core-body thermometer powered by gastric acid battery. *IEEE Sens J.* **2018**, *18*, 9755–9762.

(10) Hafezi, H.; Robertson, T. L.; Moon, G. D.; Au-Yeung, K.-Y.; Zdeblick, M. J.; Savage, G. M. An ingestible sensor for measuring medication adherence. *IEEE Trans Biomed Eng.* **2015**, *62*, 99–109.

(11) Flores, G. P.; Peace, B.; Carnes, T. C.; Baumgartner, S. L.; Buffkin, D. E., Jr; Euliano, N. R.; Smith, L. N. Performance, reliability, usability, and safety of the ID-Cap system for ingestion event monitoring in healthy volunteers: a pilot study. *Innov Clin Neurosci* **2016**, *13*, No. 12.

(12) Baumgartner, S. L.; Buffkin, D. E., Jr; Rukavina, E.; Jones, J.; Weiler, E.; Carnes, T. C. A novel digital pill system for medication adherence measurement and reporting: Usability validation study. *JMIR Hum Factors* **2021**, *8*, No. e30786.

(13) Chai, P. R.; Goodman, G.; Bustamante, M. J.; Mohamed, Y.; Castillo-Mancilla, J.; Boyer, E. W.; Mayer, K. H.; Rosen, R. K.; Baumgartner, S. L.; Buffkin, E.; et al. Long-term stability of the electronic sensor component of a digital pill system in real-world storage settings. *J. Pharm. Technol.* **2021**, *37*, 135–139.

(14) Yoshida, S.; Miyaguchi, H.; Nakamura, T. Prototyping of an all-pMOS-based cross-coupled voltage multiplier in single-well CMOS technology for energy harvesting utilizing a gastric acid battery. *Electronics* **2019**, *8*, No. 804.

(15) Yoshida, S.; Miyaguchi, H.; Nakamura, T. Development of ingestible thermometer with built-in coil antenna charged by gastric acid battery and demonstration of long-time in vivo telemetry. *IEEE Access* **2021**, *9*, 102368–102377.

(16) Kim, Y. J.; Chun, S.-E.; Whitacre, J.; Bettinger, C. J. Self-deployable current sources fabricated from edible materials. *J. Mater. Chem. B* **2013**, *1*, 3781–3788.

(17) Egan, T.; Jacquier, J.-C.; Rosenberg, Y.; Rosenberg, M. Cold-set whey protein microgels containing immobilised lipid phases to modulate matrix digestion and release of a water-soluble bioactive. *J. Microencapsul* **2014**, *31*, 184–192.

(18) Hanawa, T. Biocompatibility of titanium from the viewpoint of its surface. *Sci. Technol. Adv. Mater.* **2022**, *23*, 457–472.

(19) O'Brien, B. *Advances in Metallic Biomaterials*; Springer, 2015; pp 245–272.

(20) Fernandes, C.; Taurino, I. Biodegradable molybdenum (mo) and tungsten (w) devices: One step closer towards fully-transient biomedical implants. *Sensors* **2022**, *22*, No. 3062.

(21) Oldfield, J. W. *Galvanic Corrosion*; ASTM International, 1988.

(22) Kakaei, K.; Esrafil, M. D.; Ehsani, A. Interface Science and Technology. In *Graphene Surfaces*; Kakaei, K.; Esrafil, M. D.; Ehsani, A., Eds.; Elsevier, 2019; Vol. 27, pp 253–301.

(23) Heard, D. M.; Lennox, A. J. Electrode materials in modern organic electrochemistry. *Angew. Chem., Int. Ed. Engl.* **2020**, *59*, 18866–18884.

(24) Birke, K. P.; Schweitzer, D. N. *Modern Battery Engineering: A Comprehensive Introduction*; World Scientific, 2019; pp 1–30.

(25) Jia, X.; Yang, Y.; Wang, C.; Zhao, C.; Vijayaraghavan, R.; MacFarlane, D. R.; Forsyth, M.; Wallace, G. G. Biocompatible ionic liquid–biopolymer electrolyte-enabled thin and compact magnesium–air batteries. *ACS Appl. Mater. Interfaces* **2014**, *6*, 21110–21117.

(26) Chew, C. S. *Encyclopedia of Gastroenterology*; Elsevier, 2004; pp 105–116.

(27) Lu, P.-J.; Hsu, P.-I.; Chen, C.-H.; Hsiao, M.; Chang, W.-C.; Tseng, H.-H.; Lin, K.-H.; Chuah, S.-K.; Chen, H.-C. Gastric juice

acidity in upper gastrointestinal diseases. *World J. Gastroenterol* **2010**, *16*, No. 5496.

(28) Gennari, F. J.; Weise, W. J. Acid-base disturbances in gastrointestinal disease. *Clin J. Am. Soc. Nephrol* **2008**, *3*, 1861–1868.

(29) Hasan, B. O. Galvanic corrosion of carbon steel–brass couple in chloride containing water and the effect of different parameters. *J. Pet Sci. Eng.* **2014**, *124*, 137–145.